Applied Catalysis B: Environmental 115–116 (2012) 225–235

Contents lists available at SciVerse ScienceDirect

Applied Catalysis B: Environmental

journal homepage: www.elsevier.com/locate/apcatb

Ethanol adsorption and oxidation on bimetallic catalysts containing platinum and base metal oxide supported on MCM-41

Kamolwan Rintramee[a], Karin Föttinger[b], Günther Rupprechter[b], Jatuporn Wittayakun[a,*]

[a] School of Chemistry, Institute of Science, Suranaree University of Technology, Nakhon Ratchasima 30000, Thailand
[b] Institute of Materials Chemistry, Vienna University of Technology, 1060 Vienna, Austria

ARTICLE INFO

Article history:
Received 27 May 2011
Received in revised form 9 November 2011
Accepted 28 November 2011
Available online 8 December 2011

Keywords:
Ethanol adsorption
Ethanol oxidation
Bimetallic catalyst
MCM-41
Platinum
Cobalt

ABSTRACT

Ethanol pollutant either emitted from ethanol-fueled vehicles at low temperature or released from industries as volatile organic compound (VOC) could be removed by catalytic oxidation. This work investigated adsorption of ethanol on bimetallic catalysts containing Pt with loading of 0.5 wt% and Co, Cu, or Mn with loading of 15 wt% supported on RH-MCM-41 by temperature programmed desorption (ethanol-TPD) and thermogravimetric analysis (ethanol-TGA). Evolution of gases from the ethanol-TPD indicated the role of oxides as potential oxygen supplier in ethanol oxidation. On the monometallic catalyst containing oxides of Co, Cu, and Mn on MCM-41, the oxide of Co was the better oxygen supplier than that of the others to react with the adsorbed ethanol to produce CO_2. Furthermore, the bimetallic 0.5Pt–15Co/RH-MCM-41 with cobalt in the form of Co_3O_4, showed the highest ethanol adsorption and CO_2 desorption. Consequently, ethanol oxidation was studied on the bimetallic 0.5Pt–15Co/RH-MCM-41 by *in situ* infrared spectroscopy in which intermediates and reaction pathways were proposed when ethanol and oxygen were flowed through the cell at various temperatures. Results from the ethanol oxidation in a fixed bed flow reactor showed that the bimetallic catalyst gave lower ethanol conversion than monometallic Pt but seemed to be more stable than the monometallic Pt catalyst.

1. Introduction

Ethanol (C_2H_5OH) has been used as an additive or substitute of gasoline to improve octane number and to reduce an emission of carbon monoxide (CO) from the automotive exhaust. However, ethanol can be classified as a pollutant when it is emitted from low-efficient ethanol-fueled vehicles. Moreover, an incomplete combustion of ethanol can generate other toxic compounds such as CO and acetaldehyde (C_2H_4O). In another aspect ethanol can be thought of as a volatile organic compound (VOC) because it has been used widely in various industries, e.g. as a solvent.

An effective method to reduce ethanol is catalytic oxidation which can be operated at low temperature. In general, the products from the ethanol oxidation depend on the amount of oxygen [1]. In excess of oxygen, only a complete oxidation (Eq. (1)) is expected but it also depends on catalyst and reaction conditions. Both partial and incomplete oxidation (Eqs. (2) and (3)) should be minimized because they produce acetaldehyde and CO, respectively.

$$\text{Complete oxidation}: \quad C_2H_5OH + 3O_2 \rightarrow 2CO_2 + 3H_2O \qquad (1)$$

$$\text{Partial oxidation}: \quad C_2H_5OH + (1/2)O_2 \rightarrow CH_3CHO + H_2O \qquad (2)$$

$$\text{Incomplete oxidation}: \quad C_2H_5OH + 2O_2 \rightarrow 2CO + 3H_2O \qquad (3)$$

Noble metals such as Pt, Pd, or Rh are good catalysts for ethanol oxidation [2–5]. The study of Pt supported on silica and alumina (Pt/SiO_2 and Pt/Al_2O_3, respectively) [5] suggested that the surface of Pt nanoparticles were the active sites that could trap and accumulate oxygen for ethanol oxidation. The catalytic performance depends on the type of the support and the intermediates during the reaction could be detected by infrared spectroscopy (IR). However, the noble metal catalysts could be easily poisoned by undesired reaction intermediates such as surface ethyl from ethanol dehydration which leads to deactivation by coking [6]. In the case of CO oxidation over Pt/SiO_2, the activity of Pt can be inhibited by strong adsorption of CO but the problem could be solved by adding metal oxides to serve as oxygen source for the surface reaction [7].

Base metal oxides have been developed for ethanol oxidation because of their resistance to poisoning and lower price than noble metal. Cu/Al_2O_3 was reported to be active for oxidation of ethanol and acetaldehyde [1]. The activity varied with Cu loading and the complete oxidation was the major reaction. The CO_2 yield could be improved by mixing Cu with Cr. In addition, modification of Al_2O_3 with cerium oxide (CeO_2) before an impregnation of Cu could increase the activity for complete oxidation [8].

* Corresponding author. Tel.: +66 4422 4256; fax: +66 4422 4185.
E-mail address: jatuporn@sut.ac.th (J. Wittayakun).

0926-3373/$ – see front matter © 2011 Elsevier B.V. All rights reserved.
doi:10.1016/j.apcatb.2011.11.050

Oxides of Mn are also active for ethanol oxidation [9]. The catalytic performance depends on oxidation state of Mn and amount of the lattice oxygen. Lamaita et al. [10] reported that the activity of Mn can be related to both of their oxidation states (Mn^{3+} and Mn^{4+}) and the presence of Mn^{4+} vacancies. Adsorption of ethanol, confirmed by IR generated ethoxy species which transformed to carboxylate, acetaldehyde and CO_2. A mixed oxide catalysts such as $CuO–MnO_2$ was reported to be only slightly less active than Pt/Al_2O_3 catalyst for the same volume in the combustion of ethanol [4]. The Mn catalysts prepared from $KMnO_4$ on Al_2O_3 was active for total ethanol oxidation. The fast step was the formation of acetate species from ethanol and the slow step was the conversion of the surface acetate to CO_2. The catalytic activity of supported manganese oxides was higher than the un-supported one. The activity also depended on support type which caused variation in manganese reducibility and mobile oxygen species [11].

Recently, Rodrigues et al. [12] studied partial oxidation of ethanol on Co_3O_4 based cordierite monolith catalyst to produce synthesis gas, a mixture of CO and H_2 (Eq. (4)). The highest selectivity for CO was achieved at 770 °C whereas acetaldehyde was a major product at the temperature lower than 600 °C.

$$\text{Partial oxidation}: \quad C_2H_5OH + (1/2)O_2 \rightarrow 2CO + 3H_2 \qquad (4)$$

When a small amount of noble metal is mixed with metal oxide, the catalytic activity could be improved. For example, the addition of oxides of Co, Mn, and Ce to Pt/SiO_2 could promote the CO oxidation because the metal oxides serve as oxygen source for the surface reaction [6]. On the other hand, Pt helps metal oxides with multi-oxidation states to accelerate the oxygen transfer from gas phase to the catalyst [13]. In the elimination of CO and NO by oxidation, the temperature for $Pd–Cu/CeO_2–Al_2O_3$ catalyst in reaching 50% conversion, T_{50}, of CO was 50 °C lower than that for $Pd/CeO_2–Al_2O_3$ catalyst [14]. The role of Cu was to stabilize the zero-valence Pd.

When metals are deposited on a support with high surface area, the catalytic performance could be improved because of an improvement in metal dispersion. In this work, mesoporous MCM-41 type structure was chosen as a catalyst support because of its uniform pore system and high surface area [15,16]. There have been several reports on the improvement of catalytic performance by loading the catalysts on MCM-41. For example, when Cu–Mn was deposited on MCM-41, the catalytic activity of toluene oxidation was improved more than that on β-zeolite and SiO_2 because a better dispersion of Cu–Mn was obtained on the support with a higher surface area [17].

Study of ethanol adsorption on catalysts at conditions similar to the testing conditions could lead to more understanding on the mechanism of ethanol oxidation and the role of the metal catalysts. For examples, Yee et al. [18] studied intermediates and products of ethanol oxidation on reduced and unreduced CeO_2 and Pd/CeO_2 by Fourier transform infrared spectroscopy (FT-IR) and temperature programmed desorption (TPD). They reported an increase in dehydrogenation of ethanol to acetaldehyde in the presence of Pd. Sanchez-Sanchez et al. [19] investigated adsorbed species and products on Pt, Ni and PtNi catalysts support on Al_2O_3 with combined analysis of ethanol-TPD and diffuse reflectance Fourier transform infrared spectroscopy (DRIFT) spectra. The gas products from the PtNi bimetallic catalyst showed the lowest desorption temperature suggesting that the activity in the C—C bond rupture was higher than that of monometallic counterparts.

The goal of this work was to study adsorption and oxidation of ethanol on catalysts containing 0.5 wt% of Pt and fixed amount of Co, Cu, and Mn. The bimetallic catalysts were impregnated on MCM-41 synthesized by using rice husk silica (referred to as RH-MCM-41) to increase dispersion. Adsorption of ethanol on these catalysts was studied by temperature programmed desorption (ethanol-TPD) in the absence of air to observe the role of oxides as oxygen supplier for surface oxidation. The oxide with highest oxygen involvement was further studied for oxidation by air with *in situ* infrared spectroscopy (*in situ* IR) to identify the reaction intermediates and to understand the reaction mechanism. Finally, the ethanol oxidation by air was studied using a flow reactor to determine the catalytic performance at various temperatures.

2. Experimental

2.1. RH-MCM-41 synthesis

The RH-MCM-41 was synthesized by hydrothermal method with a procedure modified from the literature [20]. A clear solution of sodium silicate was prepared by mixing rice husk silica (3.0 g) with a NaOH solution (5 M, 30 ml prepared from pellets purchased from Carlo Erba) under stirring in a polypropylene bottle. This mixture was added to an aqueous solution of cetyltrimethyl ammonium bromide (CTAB, 0.14 M, 90 ml, prepared from solid purchased from Fluka) and stirred at room temperature for 4 h. The solution pH was adjusted to 11 by 5 N H_2SO_4 (Carlo Erba, 96% purity). The resulting mixture was transferred to a Teflon-lined stainless steel autoclave and heated at 100 °C for 3 days. The solid product, as-synthesized RH-MCM-41 was separated by centrifugation, washed thoroughly with deionized water and dried at 100 °C. Finally, the organic template was removed by calcination in atmospheric pressure at 540 °C for 6 h.

2.2. Catalyst preparation

Monometallic Pt/RH-MCM-41 with Pt loading of 0.5 wt% and M/RH-MCM-41 (M = Co, Cu, and Mn) with M loading of 15 wt% were prepared by impregnation method with a solution of $H_2PtCl_6{\cdot}6H_2O$ (Alfa), $Co(NO_3)_2{\cdot}6H_2O$ (Merck), $Cu(NO_3)_2{\cdot}3H_2O$ (Merck), and $Mn(NO_3)_2{\cdot}4H_2O$ (Merck), respectively. The samples were dried at 70 °C for 1 h and then 100 °C overnight and calcined at 500 °C for 2 h. The resulting catalysts were notated as 0.5Pt/RH-MCM-41, 15Co/RH-MCM-41, 15Cu/RH-MCM-41, and 15Mn/RH-MCM-41, respectively.

The bimetallic Pt-M/RH-MCM-41 catalysts with a 0.5 wt% Pt and 15 wt% of M were prepared by sequential impregnation method. The monometallic catalysts 15 M/RH-MCM-41, prepared as above, were impregnated with an aqueous solution of $H_2PtCl_6{\cdot}6H_2O$, dried at 70 °C for 1 h and then 100 °C overnight and calcined at 500 °C for 2 h. The catalysts were notated as 0.5Pt–15Co/RH-MCM-41, 0.5Pt–15Cu/RH-MCM-41, and 0.5Pt–15Mn/RH-MCM-41, respectively.

2.3. Catalyst characterization

Metals content of catalysts were analyzed by inductively coupled plasma mass spectroscopy (ICP-MS) with an Agilent 7500ce. A 50-mg sample was dissolved in $HCl/HNO_3/HF/H_3BO_3$ solution (0.8/1.2/0.4/6 ml of volume).

Physical characteristic of the samples were studied by nitrogen adsorption–desorption analysis at −196 °C at relative pressure from 0.01 to 0.99 on an AUTOSORB-1 analyzer. Before measurement, each sample was degassed with heat at 300 °C under vacuum for 4 h. The surface area was calculated using BET method from the adsorption data in the relative pressure range from 0.02 to 0.2. The pore size was calculated from the desorption branches of the isotherm using Barrett–Joyner–Halenda (BJH) method.

Powder XRD patterns were obtained from a Bruker axs D5005 diffractometer. The Cu K_α X-ray was generated with a current of 35 mA and a potential of 35 kV. The catalysts were scanned in two ranges 2θ low angle from 1 to 10 degrees and wide angle from 20

to 70 degrees. The powder pattern of each catalyst was recorded in the same day with the same amount, so that the intensity of the peaks could be roughly compared.

X-ray absorption near edge structure (XANES) spectra of mono- and bimetallic containing Co, Cu and Mn were recorded in a transmission mode at the Beamline 8 of the Synchrotron Light Research Institute, Thailand [21]. The storage ring was normally operated with the electron energy of 1.2 GeV and electron current between 90 and 140 mA. Using a synchrotron X-ray monochromator equipped with double Ge (2 2 0) crystals, the photon energy was scanned from 7690 to 7780 eV, 8950 to 9060 eV, and 6510 to 6620 eV for the samples containing Co, Cu and Mn, respectively. The energy calibration for scanning the X-ray energy was performed using standard foils of Co, Cu, and Mn (Exafs Material, Inc.) at their *K*-edges. The percentages of oxide phases of Co, Cu, and Mn were determined by comparing the XANES spectrum of each catalyst to those of standard materials using a Linear Combination Fitting tool available in the ATHENA program [22]. Besides the foils, the oxide standards of Co, Cu and Mn were: CoO, Co_3O_4; CuO, Cu_2O; MnO, MnO_2, Mn_2O_3; respectively.

2.4. Ethanol-TPD

The ethanol-TPD analysis was performed in a tubular flow reactor connected to a mass spectrometer (Balzers Prisma 260). First, the monometallic 15 M/RH-MCM-41 catalysts (M = Co, Cu, Mn) were tested to observe the ability of the oxides to react with adsorbed ethanol to produce CO_2. Then the 0.5Pt/RH-MCM-41 and bimetallic 0.5Pt–15M/RH-MCM-41 were studied.

In the ethanol-TPD procedure, each catalyst (50 mg) was packed between quartz wool bed in a quartz tube, heated under the flow of He (50 ml/min) at 300 °C (ramping rate of 5 °C/min) for 4 h and reduced at under a flow of H_2 (30 ml/min) at 200 °C for 2 h. Then the H_2 was switched to He (25 ml/min) to remove the adsorbed hydrogen on the catalyst. The ethanol adsorption was carried out by flowing He (25 ml/min) into a saturator containing ethanol, then through the catalyst at 30 °C for 2 h. The catalyst was purged by He (25 ml/min) at 30 °C for 4 h. The ethanol-TPD was performed at ambient temperature to 400 °C with a heating rate of 5 °C/min, held at 400 °C for 30 min. The signal of ethanol and desorbed gases were monitored by the mass spectrometer.

2.5. Ethanol adsorption by thermogravimetric analysis (ethanol-TGA)

Ethanol adsorption of each catalyst was analyzed by thermogravimetric analysis (TGA) (NETZSCH; STA 409 PC). In the TGA, the catalyst (50 mg) was pretreated by heat under a flow of N_2 (50 ml/min) from room temperature to 300 °C with a ramping rate of 5 °C/min and held for 1 h. Then, the catalyst was reduced under a flow of H_2 (30 ml/min) at 200 °C with a ramping rate of 5 °C/min. After cooled down to 30 °C, the catalyst was purged by N_2 (25 ml/min) until a constant weight was obtained. Then vapor generated by flowing N_2 through a saturator containing ethanol was flowed over the catalyst at 30 °C. When a saturated adsorption was obtained, i.e., the weight became constant, the catalyst was purged by a flow of N_2 to remove physisorbed species. Finally, the ethanol desorption was conducted under the flow of N_2 (25 ml/min) by ramping the temperature to 600 °C at 5 °C/min and then held for 1 h.

2.6. Ethanol oxidation studied by in situ infrared spectroscopy (in situ IR)

A self-support wafer (~0.6 cm diameter) of a catalyst powder was prepared by a hydraulic press, put into an *in situ* sample holder, heated under the flow of He (50 ml/min) at 300 °C with a ramping rate of 10 °C/min for 1 h and reduced under a flow of H_2 (30 ml/min) at 300 °C for 1 h. Then the H_2 was switched to He (25 ml/min) to remove hydrogen residue on the catalyst. The ethanol vapor was mixed with synthetic air and introduced to the *in situ* cell at 30 °C and heated to 300 °C with a ramping rate of 10 °C/min. The *in situ* IR spectra of species during the oxidation were recorded at 30, 100, 150, 200, 250 and 300 °C on a Bruker IFS 28 spectrometer over the 4000–1000 cm^{-1} range at a resolution of 4 cm^{-1}. The spectra were normalized using the intensity of the MCM-41 structural vibrations which was in the range 2100–1770 cm^{-1} [23].

2.7. Ethanol oxidation in a fixed bed flow reactor

Each catalyst was tested in a continuous-flow fixed bed reactor connected to a gas chromatograph (GC). Before the test, approximately 100 mg of catalyst was packed on a quartz wool bed in a quartz tube, heated under flowing He (50 ml/min) at 400 °C for 2 h and then reduced under flowing H_2 (30 ml/min) for 2 h. Ethanol vapour was generated by a syringe pump through a tube furnace which was heated at 100 °C and mixed with synthetic air (100 ml/min) before entering the reactor. The total flow rate was 100.2 ml/min. The concentration of ethanol was 1974 ppm and space velocity (SV) was 9550 h^{-1}. All of the reactor inlet and outlet lines were heated to prevent condensation and to preheat the feed. The reaction was studied from 100 to 400 °C and the gas components before and after the reaction were analyzed by GC (Hewlett-Packard 5890) equipped with a thermal conductivity detector. After the testing was complete the catalyst was cooled down to 100 °C under the feed of the reactants. The second run was conducted; the temperature was increased again and the reaction products were analyzed by the GC.

Because the products observed were both CO_2 and acetaldehyde, the ethanol conversion was calculated by using carbon balance according to Eqs. (1) and (2).

$$\%CH_3CH_2OH \text{ conversion} = \frac{(1/2)CO_2 + 1CH_3CHO}{(1/2)CO_2 + 1CH_3CHO + 1CH_3CH_2OH\,(\text{residue})}$$

3. Results and discussion

3.1. Catalyst characterization by ICP and N_2 adsorption–desorption

Metals contents in each catalyst were analyzed by ICP-MS. The results in Table 1 demonstrate that the metal loading in the catalysts prepared by the impregnation method were similar to the nominal values. N_2 adsorption–desorption isotherm of RH-MCM-41 and catalysts supported on RH-MCM-41 can be found in Fig. S1 of Supplementary data. The isotherm of RH-MCM-41 was type IV which is the characteristic of mesoporous materials [24]. The BET surface areas and average pore diameters are also presented in Table 1. When the RH-MCM-41 was loaded with metal, the surface area and average pore diameter decreased indicating that the pores of RH-MCM-41 were partially filled after impregnation [25]. In monometallic catalysts, the surface areas of 15Co/RH-MCM-41 was the lowest and the adsorbed volume in the mesopore region ($P/P_0 \sim 0.2$–0.5) decreased more than those of 15Cu/RH-MCM-41 and 15Mn/RH-MCM-41. The results suggested that blocking of mesopores occurred the most on 15Co/RH-MCM-41 as a result of large particles. The adsorption in mesopore region and the surface area of the bimetallic 0.5Pt15Co/RH-MCM-41 were higher than the monometallic one suggesting less pore blocking.

Table 1
Metal content and surface area of catalysts.

Catalysts	Metals content (%)				BET surface area (m^2/g)	Average pore size (nm)
	Pt	Co	Cu	Mn		
MCM-41	–	–	–	–	1352	3.1
15Co/RH-MCM-41	–	15.17	–	–	535	3.0
15Cu/RH-MCM-41	–	–	14.91	–	754	2.9
15Mn/RH-MCM-41	–	–	–	14.76	904	2.8
0.5Pt–15Co/RH-MCM-41	0.47	14.23	–	–	809	2.7
0.5Pt–15Cu/RH-MCM-41	0.37	–	14.80	–	807	2.6
0.5Pt–15Mn/RH-MCM-41	0.48	–	–	14.11	710	2.8
0.5Pt/RH-MCM-41	0.50	–	–	–	992	2.7

3.2. Catalyst characterization by XRD and XANES

The XRD pattern of the RH-MCM-41 support (not shown) consisted of characteristic peaks of MCM-41 similar to that in our previous work [20] with a strong peak at 2.3° and weak peaks at 3.9 and 4.6° corresponding to the (1 0 0), (1 1 0) and (2 0 0) plane of a hexagonal lattice. The XRD pattern of all mono- and bimetallic catalysts at low angle region (Fig. 1A and C) still showed characteristic peaks of MCM-41. After deposition with metal, the intensity of the main peak decreased. With metal loading as high as 15 wt%, the presence of oxides on the support surface could scattered out the X-ray resulting in lower diffracted intensity. Similar behavior was observed when 10 wt% of nanoparticles of TiO_2 were loaded on RH-MCM-41 [26]. In addition, the lower MCM-41-peak intensity and peak broadening was reported on Co/MCM-41 with Co loading 7–8 wt% due to secondary scattering and less ordered structure of MCM-41 [27]. With Co loading less than 3 wt%, Bhoware and Singh [28] reported that the peak of the (1 0 0) plane decreased as the loading of cobalt increased. In addition, the peak position of the (1 0 0) plane of the supported catalysts shifted slightly toward the higher angle suggesting that some metal oxide settled on wall or blocked at mesoporous channels of MCM-41.

The XRD patterns at high angle of all mono- and bimetallic catalysts are shown in Fig. 1B and D. The 15Co/RH-MCM-41 and 0.5Pt–15Co/RH-MCM-41 exhibited characteristic peaks of Co_3O_4 with diffraction peaks at 2θ of ca. 31°, 37°, 45°, 59° and 65° [27,JCPDS: PDF 43-1003]; the 15Cu/RH-MCM-41 and 0.5Pt–15Cu/RH-MCM-41 showed peaks corresponding to CuO around 2θ of 35°, 38° and 48° [29,JCPDS: PDF 44-706]; and the 15Mn/RH-MCM-41 and 0.5Pt–15Mn/RH-MCM-41 displayed weak peaks of β-MnO_2 or pyrolusite phase around 2θ of 28°, 37° and 57° [10,JCPDS: PDF 24-735]. The XRD patterns of all catalysts were the evidence that metal oxides were formed on RH-MCM-41.

In addition, the form of Co, Cu and Mn on RH-MCM-41 in the mono- and bimetallic samples were studied by XANES. The oxidation state of each metal could be determined from the edge shift

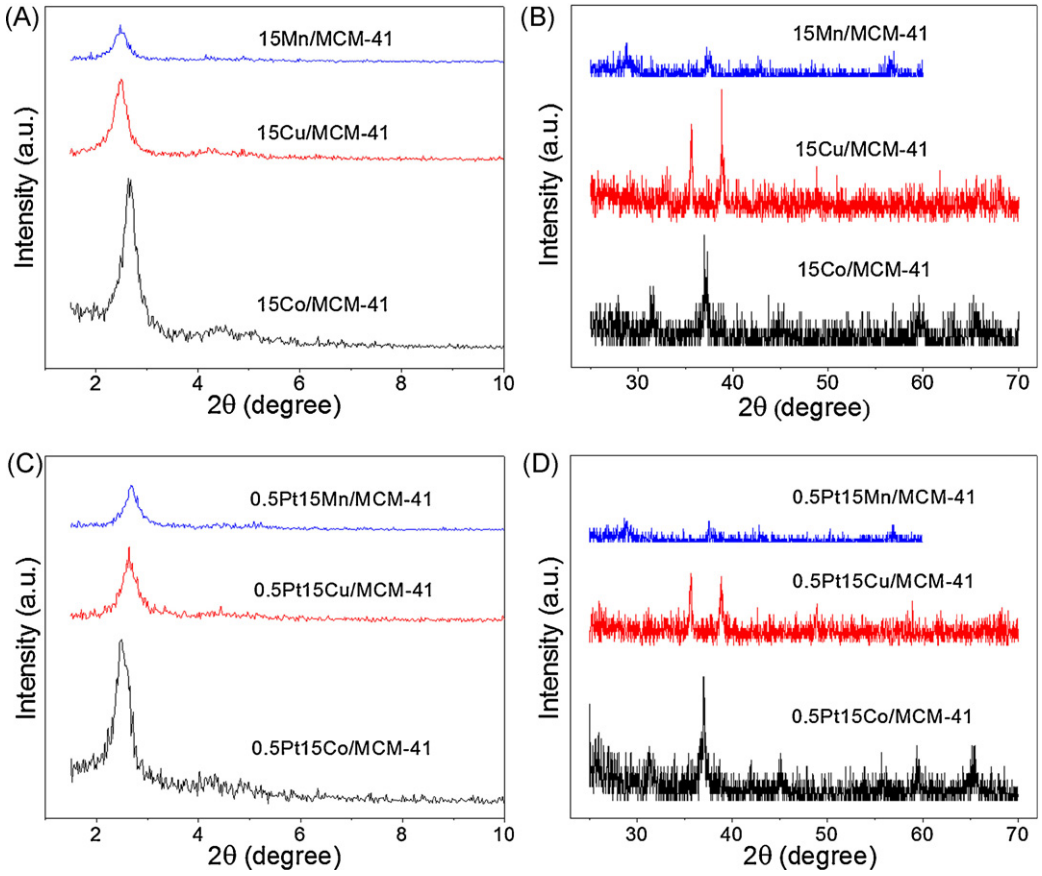

Fig. 1. XRD pattern of catalysts: (A) and (B) monometallic catalysts at low and wide angle; (C) and (D) bimetallic catalysts at low and wide angle.

Table 2
Edge energy, edge shift and oxide components in catalysts.

Catalysts	*K*-edge position (eV)	Edge shift from corresponding foil (eV)[a]	Oxide components (wt%)
15Co/RH-MCM-41	7727	18	Co_3O_4 (100%)
0.5Pt–15Co/RH-MCM-41	7727	18	Co_3O_4 (100%)
15Cu/RH-MCM-41	8991	12	CuO (100%)
0.5Pt–15Cu/RH-MCM-41	8991	12	CuO (100%)
15Mn/RH-MCM-41	6559	20	MnO_2 (90.3%), Mn_2O_3 (9.7%)
0.5Pt–15Mn/RH-MCM-41	6559	20	MnO_2 (89.8%), Mn_2O_3 (10.2%)

[a] *K*-edge of Co, Cu and Mn foil were 7709, 8979 and 6539 eV.

from that of the corresponding foil and the amount of oxide forms can be estimated by using Linear Combination Fitting of the XANES spectra. Table 2 shows the edge shifts and amount of oxide forms of each metal. The edge shifts of mono- and bimetallic were similar indicating the similar form. Exemplar of XANES spectra of Co reference materials and Co catalysts are shown in Fig. 2 and the spectra of Cu and Mn reference materials and catalysts can be found in Figs. S2 and S3 of Supplementary data, respectively. The edge shift and linear combination fitting corroborated that Co_3O_4 was the only oxide form in the Co catalysts; CuO was the only form in the Cu catalysts; and MnO_2 was the major form in Mn catalysts. The oxide forms suggested by the XANES results were consistent with the XRD results.

3.3. Ethanol-TPD

In the ethanol-TPD analysis in the absence of air, the desorbed species were detected by mass spectrometer (MS). The recorded MS fragments from possible desorbed species had *m*/*e*, ranging from the highest intensity, for examples, ethanol, 31, 45, 46, and 29; acetaldehyde, 29, 44, 43, and 15; and CO_2, 44, 28, and 16. For simplicity in the following figures, only the most intense peak of each species was displayed; the existence of other peaks was used to assist the identification. Although the fraction with *m*/*e* of 44 could be from either acetaldehyde or CO_2, it was reported that desorption of CO_2 occurred at above 300 °C [25]. Consequently, the position at low temperature was assigned to acetaldehyde and that at above 300 °C was assigned to CO_2.

The main desorbed species from all catalysts were ethanol followed by acetaldehyde; both were observed at around 100 °C. The results implied that ethanol adsorbed associatively (i.e., without any bond cleavage) on all catalysts (see the adsorption mode 1 in Scheme 1). This adsorbed species could desorb as molecular ethanol or convert simultaneously to other surface species including acetaldehyde precursors. Desorption of acetaldehyde occurred through ethanol dehydrogenation by breaking the O—H bond to produce ethoxy species (see the adsorption mode 2 in Scheme 1). Further arrangement to remove another hydrogen atom resulted in acetaldehyde. TPD profile on bare RH-MCM-41 (Fig. 3) shows ethanol desorption peaks at 100 and 250 °C. The result suggested that there were two types of adsorption sites on RH-MCM-41 and the interactions were possibly via hydrogen bond with silanol groups (Si—OH). Zhao et al. [30] studied types of silanol groups on MCM-41 by using pyridine-TPD and reported the desorption activation energies of 54.2 and 91.4 kJ/mol from hydrogen-bonded (SiOH—OHSi) and free SiOH groups, respectively. In addition, a small amount of ethylene (C_2H_4) was detected at 400 °C as a result from dehydration of ethanol adsorbed on acid sites [11]. The reaction occurred via a dissociative adsorption of ethanol via C—O bond cleavage, as shown in the third adsorption mode in Scheme 1 to produce surface ethyl and hydroxyl groups. Trawczyński et al. [11] reported that an acidic support like Al_2O_3 has high acid sites which facilitate the formation of diethyl ether and/or ethylene via dehydration of ethanol. In contrast, titania (TiO_2) which is a weak acid support generated only negligible amounts of these compounds. Because the siliceous of RH-MCM-41 in this work contained only weakly acidic silanol groups [31], only a small amount of C_2H_4 was detected. When metal precursors were deposited on RH-MCM-41, metal ions interacted with acid site of RH-MCM-41. Therefore, acid sites decreased and the products from dehydration were not observed in the TPD results.

After reduced at 200 °C, Pt species on the catalyst was likely converted to metallic form which is active for dissociative adsorption of ethanol by breaking C—O and C—C bonds [32] (adsorption mode 3 and 4 in Scheme 1). From C—O bond breaking, ethylene and water could be attributed as ethanol dehydration products. From C—C bond breaking generated CO, CH_4 and H_2 could be attributed as ethanol decomposition products. The availability of hydrogen could be responsible for hydrogenation of the surface ethylene which produced C_2H_6 as detected in the ethanol-TPD of Pt catalyst at high temperature (Fig. 4).

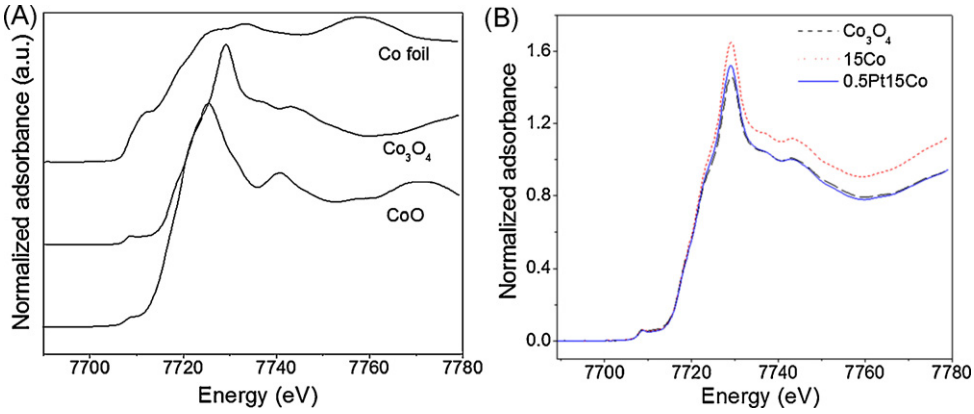

Fig. 2. The XANES spectra of Co reference materials (A) and 15Co and 0.5Pt15Co/RH-MCM-41 catalysts compare with Co_3O_4 standard (B).

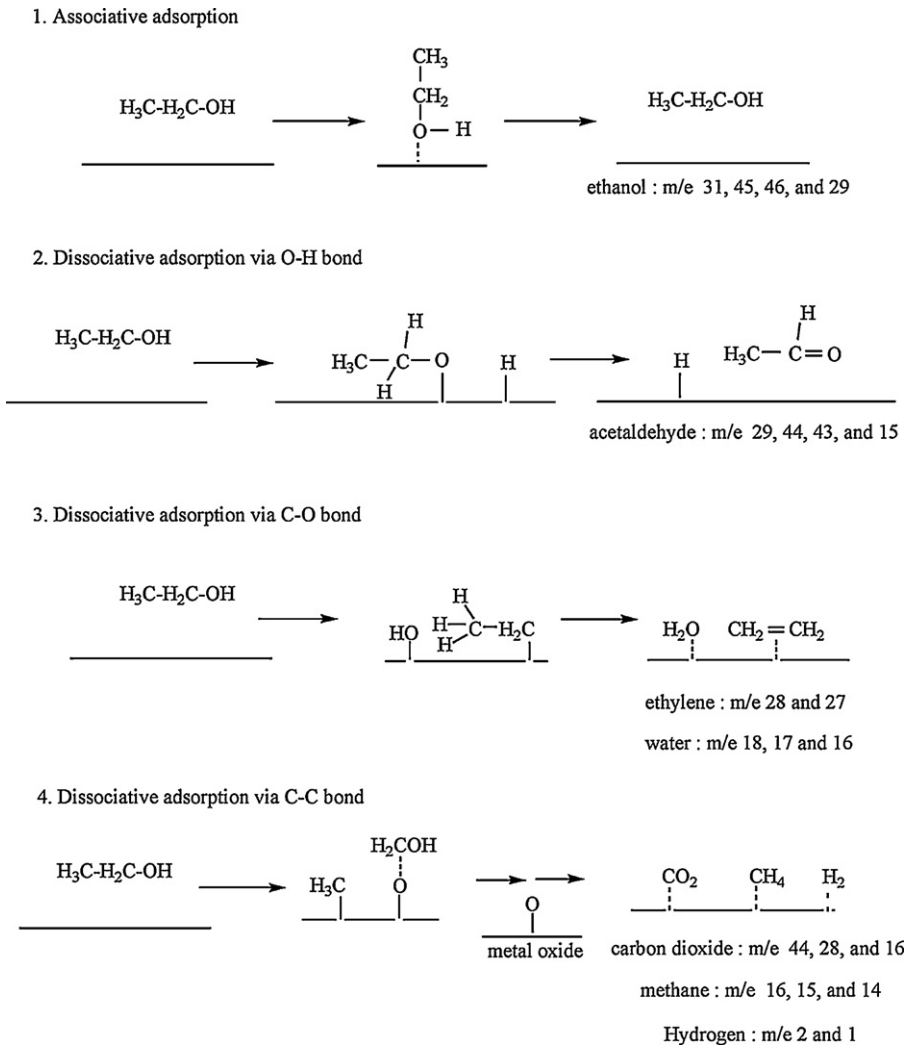

Scheme 1. Possible adsorption modes of ethanol and surface species derived from results from ethanol-TPD with mass spectrometer.

On the monometallic 15Co/MCM-41, the decomposition products and CO_2 were detected in the ethanol-TPD profile (Fig. 5A). These products could be derived from decomposition of ethanol and/or acetaldehyde. The adsorption could be through a cleavage of the C—C bond and generated $-CH_2OH$ surface species which was further converted to CO_2 at 300–400 °C (adsorption mode 4 in Scheme 1).

Ethanol-TPD profiles of 15Mn/MCM-41 (Fig. 5B) only show a small amount of CO_2 while that of 15Cu/MCM-41 (Fig. 5C) did not show any CO_2 peaks. In addition, CH_4 was not observed on both

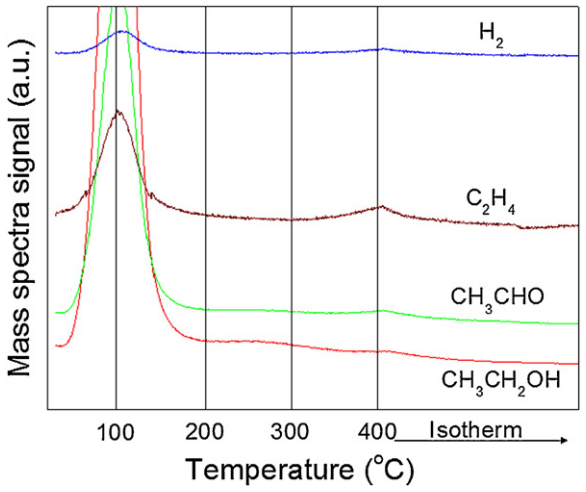

Fig. 3. Ethanol-TPD profiles on RH-MCM-41.

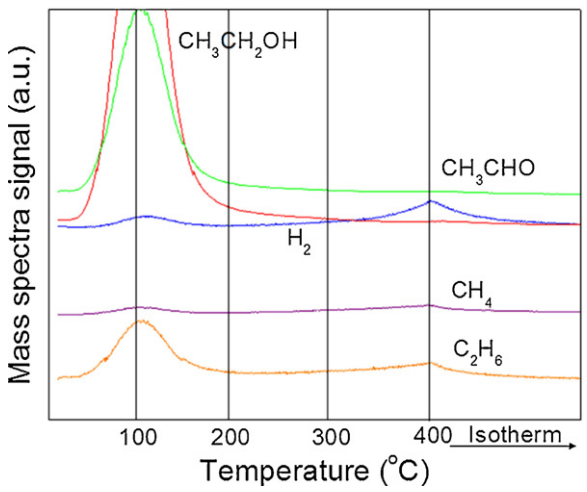

Fig. 4. Ethanol-TPD profiles on 0.5Pt/RH-MCM-41.

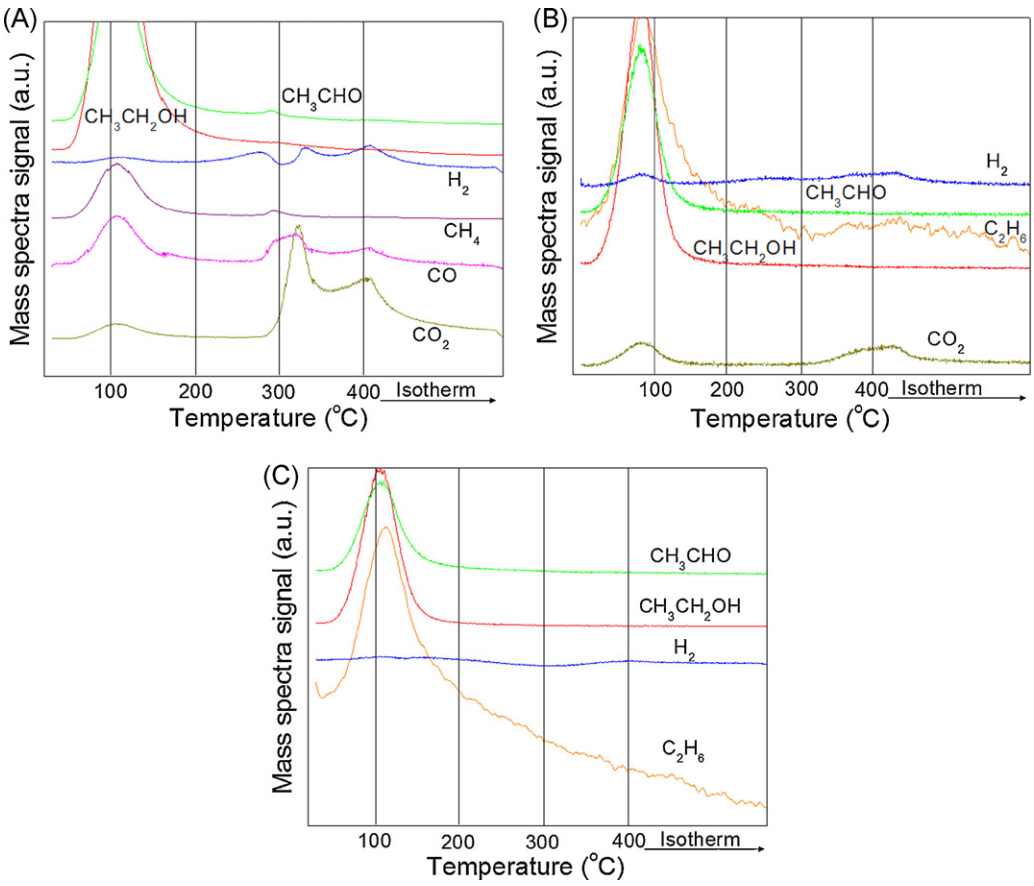

Fig. 5. Ethanol-TPD profiles on 15Co/RH-MCM-41 (A), 15Mn/RH-MCM-41 (B) and 15Cu/RH-MCM-41 (C).

catalysts, so they were not active for the rupture of ethanol molecule. Before the ethanol-TPD experiment, all catalysts were reduced by H_2 at 200 °C. In such condition Cu in both mono- and bimetallic catalysts would be converted to metallic form which was not active [33]. In contrast, Co and Mn were still mainly in oxide forms [34,35] and could supply oxygen for ethanol oxidation to generate CO_2. The form of Mn in 15Mn/RH-MCM-41 was mainly MnO_2 as confirmed by XRD and XANES results. This form was not active for ethanol oxidation [10] and, therefore, only a small amount of CO_2 was observed on the Mn catalysts.

Because CO_2 was clearly produced on 15Co/RH-MCM-41, only the ethanol-TPD of bimetallic 0.5Pt15Co/RH-MCM-41 was further discussed. The ethanol-TPD of 0.5Pt15Co/RH-MCM-41 (Fig. 6) revealed the formation of CH_4, CO, CO_2 and H_2 similar to that of 15Co/RH-MCM-41. The similarity could be a result from the similar form of Co in both catalysts. From these results, only the catalysts containing oxides of cobalt were studied by *in situ* IR and in the flow reactor.

3.4. Ethanol-TGA

The results from ethanol-TGA, also in the absence of air are shown in Table 3. The amount of ethanol adsorbed on RH-MCM-41 and all catalysts were in the range of 4.7–6.3 wt%. The RH-MCM-41 support adsorbed ethanol by using silanol groups [30]. Although all catalysts had lower surface area than RH-MCM-41, they showed higher ethanol adsorption than RH-MCM-41 indicating that ethanol also adsorbed on the metal and metal oxides. Although the Co and Pt loading were quite different, the amount of ethanol adsorbed on 15Co/RH-MCM-41 was nearly the same as that on 0.5Pt/RH-MCM-41. Because the reduction temperature in this analysis was only 200 °C, only Pt was completely reduced [36] and served as the ethanol adsorption sites. In contrast, cobalt would be reduced only partially and the adsorption occurred on the oxides. The presence of XRD peaks indicated poor dispersion which was responsible for low adsorption sites. In addition, the amount of ethanol adsorbed on 0.5Pt–15Co/RH-MCM-41 was higher than that on 15Co/RH-MCM-41 confirming that ethanol adsorbed on both Pt and cobalt oxides. These results were consistent with those from the ethanol-TPD.

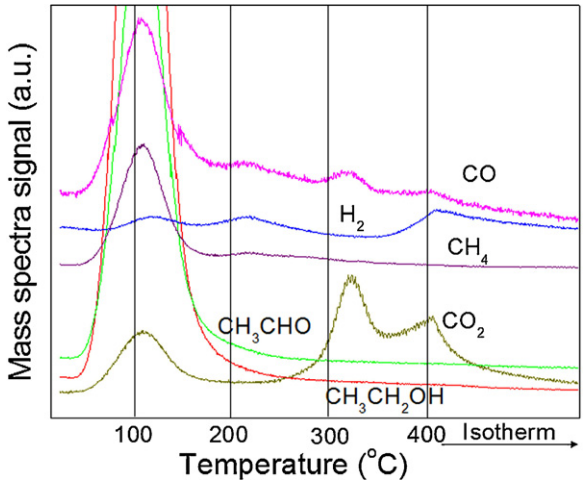

Fig. 6. Ethanol-TPD profiles on 0.5Pt–15Co/RH-MCM-41.

Table 3
Change of catalysts weight from ethanol adsorption from ethanol-TGA.

Sample after reduced at 200 °C	Catalysts weight (mg)	Weight gain (mg)	Ethanol adsorption (wt%)
RH-MCM-41	45.1	2.1	4.7
0.5Pt/RH-MCM-41	49.3	2.8	5.7
15Co/RH-MCM-41	49.8	2.9	5.8
0.5Pt–15Co/RH-MCM-41	49.3	3.1	6.3

3.5. Ethanol oxidation studied by in situ IR

The information obtained during ethanol oxidation from *in situ* IR was useful for the elaboration of reaction mechanism on the catalyst surface. After the mixture of ethanol vapor and air was passed through the catalysts at 30–300 °C, the *in situ* IR spectra of 0.5Pt/RH-MCM-41 and 0.5Pt–15Co/RH-MCM-41 were collected. Fig. 7 shows spectrum of 0.5Pt/RH-MCM-41 (Fig. 7A) and 0.5Pt–15Co/RH-MCM-41 (Fig. 7B). Spectrum (a) was recorded before an exposure to the reactant stream and spectrum (b)–(g) were recorded after an exposure to a mixture of ethanol and air from room temperature to 300 °C. The band assignments of the corresponding vibration modes and cited references are listed in Table 4. The spectrum from both samples had several similarities. The band at 1969 and 1875 cm^{-1} was assigned to overtones of lattice vibrations of RH-MCM-41 structure [23]. At the beginning (spectrum b in Fig. 7A and B), a broad band in the range of 3015–3640 cm^{-1} corresponding to the ethanol hydroxyl group was clearly observed because the surface was saturated with ethanol. At increased temperature, the band diminished allowing the observation of a sharp band at 3688 and 3711 cm^{-1} corresponding to silanol groups on the surface of both samples. A strong vibration band of Si—O—Si in the spectrum of both samples was observed at 1266 and 1250 cm^{-1}, respectively. The peaks of both catalysts before the ethanol reaction contained bands at 2338–2375 cm^{-1} indicating the presence of CO_2, thus, this CO_2 was not from the reaction. The broad bands at region 3650–3010 cm^{-1} could be attributed to stretching modes of hydroxyl group (—OH) of ethanol that adsorbed over the support and metal [37]. Those bands decreased with the temperature indicating that physisorbed ethanol was removed from the surface or changed to other species.

The *in situ* IR result could show intermediate species over surface of catalyst. Fig. 8 showed IR spectra during ethanol oxidation on both catalysts at low and high temperature. These figures could explain clearly mechanism of both catalysts. In the 0.5Pt/RH-MCM-41 case (Fig. 8A), the band of ethoxy species and acetaldehyde were observed at 30 °C after the catalyst was exposed to a stream of ethanol and air. The bands at region 2980–2875 cm^{-1} were attributed to stretching vibration of $-CH_3$ and $-CH_2-$ groups of ethoxy species. These bands gradually decreased with the temperature indicating the desorption of molecular ethanol as well as transformation to other species. The band at 1719 cm^{-1} was attributed to stretching vibration of carbonyl of acetaldehyde. This band was the most intense at 100 °C (Fig. 8B), gradually decreased with the temperature, merged with the peak at 1735 cm^{-1} and was nearly unobservable at 300 °C. These results indicated that acetaldehyde was an intermediate of ethanol oxidation produced at low temperatures from the ethoxy species and converted to other species at high temperatures. The band at 1735 and 1375 cm^{-1} were assigned to carbonyl of monodentate acetate species which could be observed at 150 °C and clearly visible at 200 (Fig. 8C) and 250 °C. In addition weak bands corresponding to bidentate acetate species were observed at 1560 and 1438 cm^{-1}. From the above result, the mechanism of ethanol oxidation over 0.5Pt/RH-MCM-41 was proposed in Scheme 2. First, ethanol adsorbed on the catalysts through its hydroxyl group to form ethoxy species, rearranged

Table 4
Band assignments and vibration modes of catalyst supported on RH-MCM-41.

Wavenumber (cm^{-1})		Assignment	Ref.
0.5Pt	0.5Pt–15Co		
Species groups on silica surface			
3688	3711	Si—OH outside channel (ν OH) (sharp)	[31]
1266	1250	Si—O—Si	[39]
3016–3625	3016–3641	(ν OH) of ethanol molecule physisorption over catalysts	[37]
Ethoxy species			[37]
2980	2977	ν_{as} CH_3	
2945	2938	ν_{as} CH_2	
2913	2906	ν_s CH_3	
2875	2875	ν_s CH_2 (shoulder)	
1484	1484	δ_{as} CH_2	
1454	1454	δ_{as} CH_3	
1391	1398	δ_s CH_3	
Acetate species			
1735	–	ν_{as} CO (monodentate acetate species)	[38]
1560	1563	ν_{as} OCO (bidentate acetate species)	[40,41]
1438	1438	ν_s OCO (bidentate acetate species)	[40,41]
–	1344	δ CH_3 (bidentate acetate species)	[40,41]
1375	–	ν_s CO (monodentate acetate species)	[38]
Acetaldehyde			
1719	–	ν CO	[42]
CO_2 physisorption			[41]
2363	2375		
2338	2344		
H_2O_{ad}			
1625	1633	(δ OH)	[43]

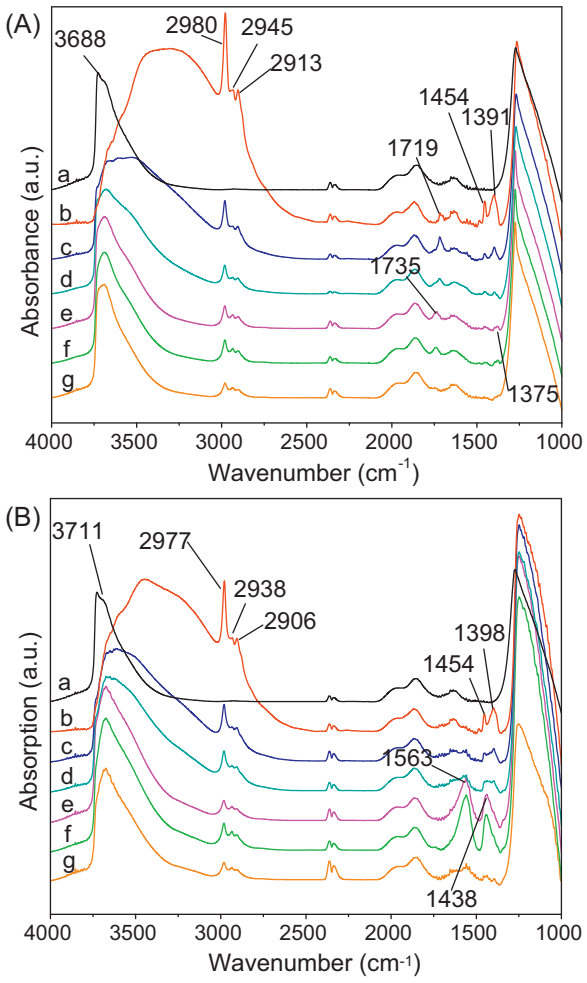

Fig. 7. *In situ* IR spectra measured on 0.5Pt/RH-MCM-41 (A) and 0.5Pt–15Co/RH-MCM-41 (B) during ethanol oxidation. Spectrum of both samples were recorded at (a) 30 °C (without ethanol and air), (b)–(g) at 30, 100, 150, 200, 250 and 300 °C, respectively (with a mixture of ethanol and air).

on the surface to form parallel adsorbed acetaldehyde [38], transformed to monodentate acetate with surface oxygen, and finally dissociated/desorbed as products (CO_2 and H_2O).

The *in situ* IR spectrum of 0.5Pt–15Co/RH-MCM-41 showed several similar features to those of the 0.5Pt/RH-MCM-41. However, the characteristic bands of acetaldehyde were not observed. The strong bands at 1563 and 1438 cm^{-1} were assigned to asymmetric and symmetric stretching modes of bidentate acetate species that were observed start on 100 °C (Fig. 8B). They were clearly observed at 200 (Fig. 8C) and 250 °C, much stronger than those in the 0.5Pt/RH-MCM-41. At 300 °C, the band of the bidentate acetate decreased significantly and the bands corresponding to CO_2 increased. The results indicated that the bidentate acetate could generate CO_2. The CO_2 bands from 0.5Pt–15Co/RH-MCM-41 were more intense than that from 0.5Pt/RH-MCM-41 possibly because there was more oxygen supply from oxides of Co for the oxidation. The mechanism of ethanol oxidation on 0.5Pt15Co/RH-MCM-41 is shown in Scheme 3. The surface ethoxy species reacted with surface oxygen to form bidentate acetate which reacted further with the surface oxygen to produce CO_2.

3.6. Ethanol oxidation in a flow reactor

The ethanol conversions from the catalytic oxidation over fresh monometallic 0.5Pt/RH-MCM-41 and bimetallic 0.5Pt–15Co/

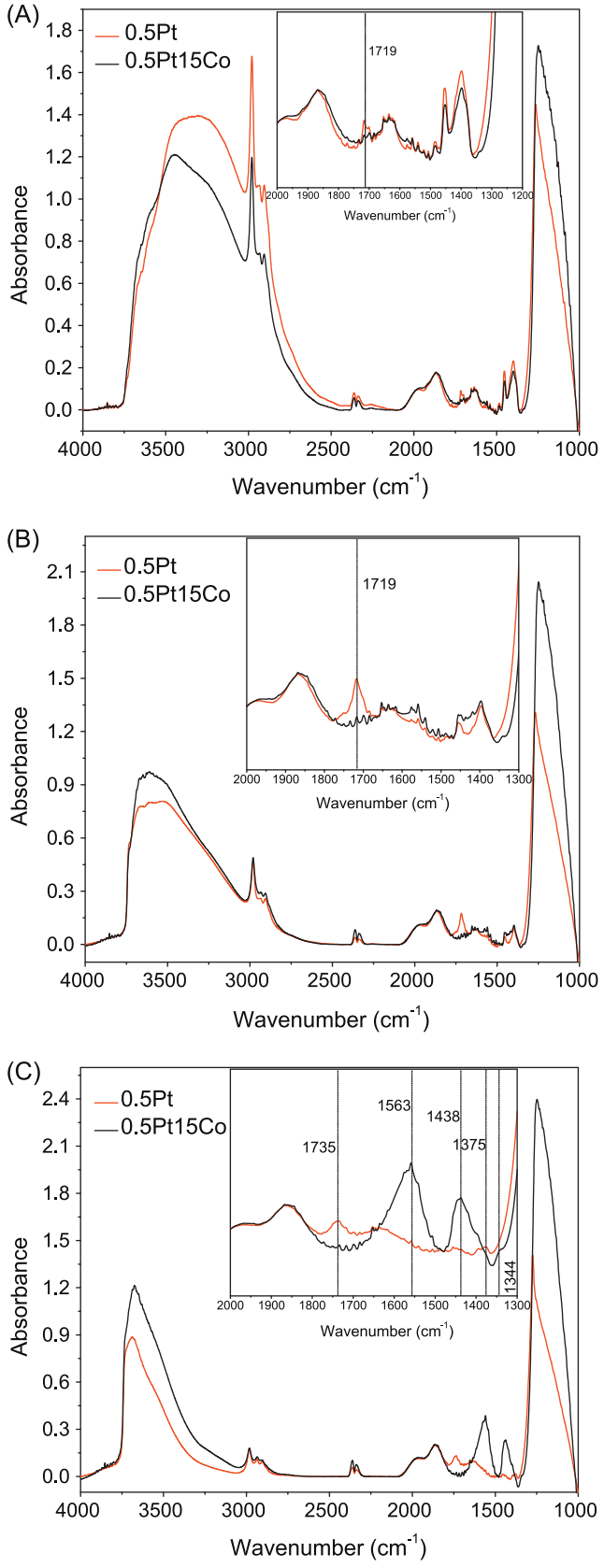

Fig. 8. *In situ* IR spectra measured on 0.5Pt/RH-MCM-41 (red line) and 0.5Pt–15Co/RH-MCM-41 (black line) during ethanol oxidation at 30 °C (A), 100 °C (B) and 200 °C (C). (For interpretation of the references to color in this figure legend, the reader is referred to the web version of this article.)

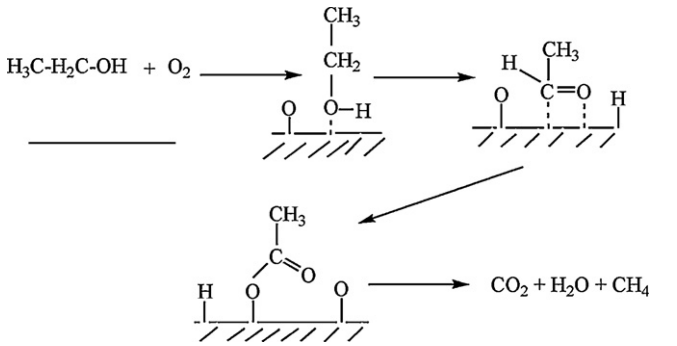

Scheme 2. Proposed mechanism of ethanol oxidation on 0.5Pt/RH-MCM-41 from *in situ* IR results.

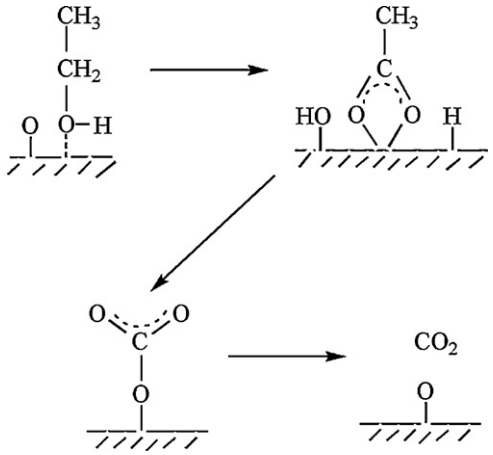

Scheme 3. Proposed mechanism of ethanol oxidation on 0.5Pt15Co/RH-MCM-41 from *in situ* IR results.

RH-MCM-41 are shown in Fig. 9A. After the first test, the reactor was cooled down to 100 °C under the flow of reactants and the second test was conducted. On both catalysts, the conversion from the first test (solid line) was not different from the second one (dash line) indicating that the catalysts were not deactivated. The conversions on both catalysts increased with temperature and were complete at high temperature. The $T_{50\%}$, the temperature for 50% ethanol conversion, of 0.5Pt/RH-MCM-41 was the lower than that of the bimetallic catalyst suggesting that the Pt catalyst was more active.

The yields of CO_2 and acetaldehyde from the catalytic oxidation over fresh monometallic 0.5Pt/RH-MCM-41 and bimetallic 0.5Pt–15Co/RH-MCM-41, calculated based on calibration curve of both products, are shown in Fig. 9B and C respectively. The CO_2 yields increased with temperature but decreased after 300 °C. The yields were not 100% suggesting that incomplete oxidation could also take place. However, the analysis of CO, the product from incomplete reaction, by GC in the work was limited due to an overlap of the peak with that of air. There were also other possibilities, for example, CO_2 could be converted to CO by using H_2 from ethanol decomposition [44]. In the second run, the CO_2 yield decreased on both catalysts but more significant on the monometallic catalyst probably because of less available oxygen on the surface. Although the yields of acetaldehyde from the fresh 0.5Pt/RH-MCM-41 were

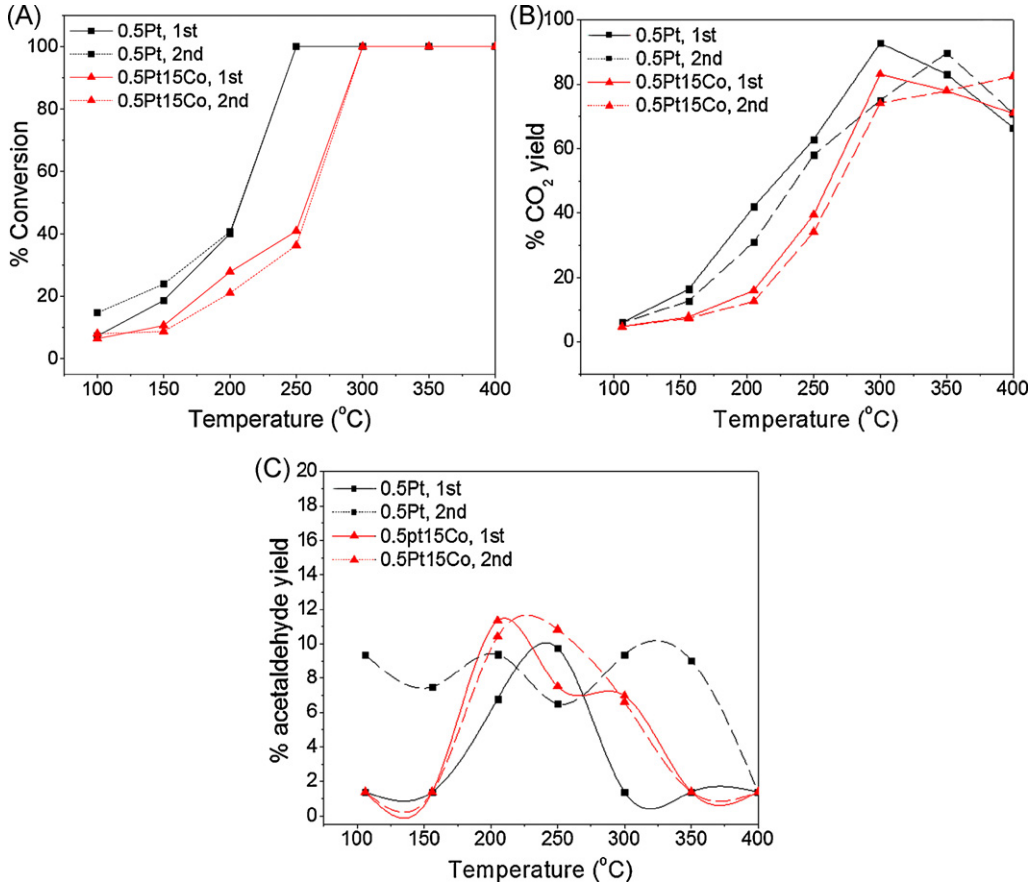

Fig. 9. Catalytic performance on 0.5Pt/RH-MCM-41 and 0.5Pt15Co/RH-MCM-41. (A) Percent of ethanol conversion, (B) Percent yield of CO_2, and (C) Percent yield of acetaldehyde; solid line: first run and dash line: second run.

observed only at 200 and 250 °C, they were observed at all temperatures in the second run. This results were consistent with the IR spectra that showed acetaldehyde intermediate specie on 0.5Pt/RH-MCM-41. Thus, the monometallic Pt catalyst was susceptible to the reaction condition and likely to be deactivated easily if tested for several times. On the other hand, the yields of acetaldehyde on the bimetallic 0.5Pt–15Co/RH-MCM-41 from the first and second runs were similar implying that the co-existence of Pt and Co on the same support could maintain the catalyst stability.

4. Conclusion

Bimetallic catalysts containing 0.5 wt% Pt and 15 wt% oxides of Co, Cu or Mn supported on RH-MCM-41 were prepared by sequential impregnation. The presence of Co_3O_4, CuO and MnO_2 were confirmed by XRD and XANES. From ethanol-TPD, the Co_3O_4 showed the highest potential as an oxygen source for ethanol oxidation after reduction at 200 °C. Cu catalyst could be Cu metallic form while MnO_2 form of Mn catalyst was inactive. Therefore, the both of catalysts are not suitable for the use as oxygen-source for the ethanol oxidation. Thus, the bimetallic Pt–Co catalyst was further studied for ethanol oxidation. The *in situ* IR result showed bidentate acetate intermediate specie over 0.5Pt–15Co/RH-MCM-41; this specie could convert to CO_2 quickly. While acetaldehyde and monodentate acetate intermediate specie was observed on 0.5Pt/RH-MCM-41 during ethanol oxidation. In the ethanol oxidation in a fixed bed flow reactor, the conversion over all catalysts increased with the temperature and CO_2 was the major product. Acetaldehyde was observed in both catalysts but more on the monometallic 0.5Pt/RH-MCM-41. The incorporation of Co_3O_4 could serve as oxygen source for catalytic ethanol oxidation and could be possible to apply to other VOC pollutants.

Acknowledgment

Scholarship for K. Rintramee is from (1) The Office of the Higher Education Commission, Thailand, under the program Strategic Scholarships for Frontier Research Network and (2) Suranaree University of Technology.

Appendix A. Supplementary data

Supplementary data associated with this article can be found, in the online version, at doi:10.1016/j.apcatb.2011.11.050.

References

[1] H. Rajesh, U.S. Ozkan, Ind. Eng. Chem. Res. 32 (1993) 1622–1630.
[2] Y.F.Y. Yao, Ind. Eng. Chem. Process Des. Dev. 23 (1984) 60–67.
[3] R.W. McCabe, P.J. Mitchell, Ind. Eng. Chem. Prod. Res. Dev. 22 (1983) 212–217.
[4] R.W. McCabe, P.J. Mitchell, Ind. Eng. Chem. Prod. Res. Dev. 23 (1984) 196–202.
[5] L.M. Petkovic, S.N. Rashkeev, D.M. Ginosar, Catal. Today 147 (2009) 107–114.
[6] L. Chen, C.K.S. Choong, Z. Zhong, L. Huang, T.P. Ang, L. Hong, J. Lin, J. Catal. 276 (2010) 197–200.
[7] Y.J. Mergler, A. van Aalst, J. van Delft, B.E. Nieuwenhuys, Appl. Catal. B: Environ. 10 (1996) 245–261.
[8] P.O. Larsson, A. Andersson, Appl. Catal. B: Environ. 24 (2000) 175–192.
[9] S.S.T. Bastos, J.J.M. Órfão, M.M.A. Freitas, M.F.R. Pereira, J.L. Figueiredo, Appl. Catal. B: Environ. 93 (2009) 30–37.
[10] L. Lamaita, M.A. Peluso, J.E. Sambeth, H.J. Thomas, Appl. Catal. B: Environ. 61 (2005) 114–119.
[11] J. Trawczynski, B. Bielak, W. Miśta, Appl. Catal. B: Environ. 55 (2005) 277–285.
[12] C.P. Rodrigues, V.T. da Silva, M. Schmal, Appl. Catal. B: Environ. 96 (2010) 1–9.
[13] J.C. Ménézo, J. Rivière, J. Barbier, React. Kinet. Catal. Lett. 49 (1993) 293–298.
[14] M. Fernández-García, A. Martínez-Arias, C. Belver, J.A. Anderson, J.C. Conesca, J. Soria, J. Catal. 190 (2000) 387–395.
[15] J.S. Beck, J.C. Vartuli, W.J. Roth, M.E. Leonowicz, C.T. Kresge, K.D. Schmitt, C.T.W. Chu, D.H. Olson, E.W. Sheppard, J. Am. Chem. Soc. 114 (1992) 10834–10843.
[16] P. Selvam, S.K. Bhatia, C.G. Sonwane, Ind. Eng. Chem. Res. 40 (2001) 3237–3261.
[17] W.B. Li, M. Zhuang, T.C. Xiao, M.L.H. Green, J. Phys. Chem. B 110 (2006) 21568–21571.
[18] A. Yee, S.J. Morrison, H. Idriss, J. Catal. 191 (2000) 30–45.
[19] M.C. Sanchez-Sanchez, R.M.N. Yerga, D.I. Kondarides, X.E. Verykios, J.L.G. Fierro, J. Phys. Chem. A 114 (2010) 3873–3882.
[20] J. Chumee, N. Grisdanurak, A. Neramittagapong, J. Wittayakun, Sci. Technol. Adv. Mater. 10 (2009) 1–6.
[21] W. Klysubun, P. Sombunchoo, N. Wongprachanukul, P. Tarawarakarn, S. Klinkhieo, J. Chaiprapa, P. Songsiriritthigul, Nucl. Instrum. Methods Phys. Res. Sect. A 582 (2007) 87–89.
[22] B. Ravel, M. Newville, J. Synchrotron Radiat. 12 (2005) 537–541.
[23] J.P. Bellat, O. Bertrand, F. Bouvier, M. Broyer, V. Frangois, S. Maure, G. Weber, Stud. Surf. Sci. Catal. 125 (1999) 737–744.
[24] K.M. Parida, S.S. Dash, J. Mol. Catal. A: Chem. 306 (2009) 54–61.
[25] X. Xu, C. Song, J.M. Andresen, B.G. Miller, A.W. Scaroni, Energy Fuels 16 (2002) 1463–1469.
[26] S. Artkla, W. Kim, W. Choi, J. Wittayakun, Appl. Catal. B: Environ. 91 (2009) 157–164.
[27] J. Panpranot, S. Kaewkuna, P. Praserthdam, J.G. Goodwin, Catal. Lett. 91 (2003) 1–2.
[28] S.S. Bhoware, A.P. Singh, J. Mol. Catal. A: Chem. 266 (2007) 118–130.
[29] Z.Y. Wu, Y.M. Wang, J.H. Zhu, Studies Stud. Surf. Sci. Catal. 156 (2005) 139–146.
[30] X.S. Zhao, G.Q. Lu, A.K. Whittaker, G.J. Millar, H.Y. Zhu, J. Phys. Chem. B 101 (1997) 6525–6531.
[31] A. Jentys, K. Kleestorfer, H. Vinek, Micropor. Mesopor. Mater. 27 (1999) 321–328.
[32] S.M. Lima, A.M. Silva, U.M. Graham, G. Jacobs, B.H. Davis, L.V. Mattos, F.B. Noronha, Appl. Catal. A: Gen. 352 (2009) 95–113.
[33] T. Tsoncheva, J. Rosenholm, M. Linden, L. Ivanova, C. Minchev, Appl. Catal. A: Gen. 318 (2007) 234–243.
[34] T. Tsoncheva, L. Ivanova, J. Rosenholm, M. Linden, Appl. Catal. B: Environ. 89 (2009) 365–374.
[35] H. Pérez, P. Navarro, J.J. Delgado, M. Montes, Appl. Catal. A: Gen. 400 (2011) 238–248.
[36] I. Sobczak, M. Ziolek, M. Nowacka, Micropor. Mesopor. Mater. 78 (2005) 103–116.
[37] O. Akdim, W. Cai, V. Fierro, H. Provendier, A. van Veen, W. Shen, C. Mirodatos, Top. Catal. 51 (2008) 22–38.
[38] M. Nagal, R.D. Gonzalez, Ind. Eng. Chem. Prod. Res. Dev. 24 (1985) 525–531.
[39] K. Haga, H. Watanabe, J. Non-Cryst. Solids 195 (1996) 72–75.
[40] A. Yee, S.J. Morrison, H. Idriss, J. Catal. 186 (1999) 279–295.
[41] H. Song, U.S. OZkan, J. Catal. 261 (2009) 66–74.
[42] M. Scott, M. Goeffroy, W. Chiu, M.A. Blackford, H. Idriss, Top. Catal. 51 (2008) 13–21.
[43] Z. Yu, S.S.C. Chuang, J. Catal. 246 (2007) 118–126.
[44] A. Therdthianwong, T. Sakulkoakiet, S. Therdthianwong, ScienceAsia 27 (2001) 193–198.